Numerical Investigation of Erosion Due to Particles in a Cavitating Flow in Pelton Turbine

Luka Kevorkijan¹ – Matjaž Hriberšek¹ – Luka Lešnik¹ – Aljaž Škerlavaj² – Ignacijo Biluš¹ ⊠

- 1 University of Maribor, Faculty of Mechanical Engineering, Slovenia
- 2 Scotta Turboinštitut, Slovenia

ignacijo.bilus@um.si

Abstract Erosion of Pelton turbine components due to cavitation and particle-laden flow is a major challenge in hydropower applications, particularly in sediment-rich river environments. This study presents a numerical investigation on how solid particles contribute to the erosion of a Pelton runner. Computational fluid dynamics (CFD) simulations were conducted using ANSYS CFX 2023 R2, incorporating a Lagrangian particle tracking approach and the Finnie abrasion model to predict erosion patterns under varying sediment concentrations. The results indicate that, under normal sediment conditions, particle erosion does not significantly contribute to blade tip damage. However, under extreme sediment loading, the predicted erosion patterns closely match real-world observations, particularly at the blade tip.

Keywords Pelton turbine, solid particle erosion, cavitation, CFD simulation

Highlights

- Numerical CFD analyzis was used to evaluate erosion in Pelton turbine runners.
- Particle erosion is negligible under normal sediment conditions but significant under extreme loading.
- Erosion patterns predicted by simulations align with real-world turbine wear.

1 INTRODUCTION

Multiphase flows occur in wide range of devices in process and energy engineering. In some cases, their occurrence is intentional due to the process taking place between the phases in the flow, such as in spray coating (spray towers), preparation of suspensions in the pharmaceutical and food industries (fluidized bed devices, mixing reactors), distillation, drying, air conditioning (air conditioning and ventilation systems), combustion in thermal machines (thermal power plants, internal combustion engines), coating removal (sandblasting), and many other processes [1].

However, multiphase flow can also arise unintentionally as a consequence of natural phenomena or engineering process, for example, solid particles in emissions during combustion (combustion in internal combustion engines, thermal power plants, fires), sediments in river flows (flow through hydraulic turbine machines) and sand particles in wind flow (wind erosion in deserts).

In general, multiphase flows are classified into stratified and dispersed types, with flows containing solid dispersed phases, such as particles in liquid flow, being a special case of the latter. Due to the frequent occurrence of such flows in process and energy devices, the interaction of particles with the walls of the devices is of significant engineering interest. These interactions can result in material loss from the wall surface, commonly referred to as abrasion. A particularly relevant issue is the damage to the flow components of turbine machines operating in rivers polluted with sediments [2].

In 2023, approximately 750 million people worldwide still lacked access to electricity [3]. In the preceding year, 4300 TWh of electricity worldwide was produced in hydropower plants, accounting for about 15 % of total global electricity production. Annual growth of production was 2 %, with projections suggesting an increase of 4 % by 2030 [4].

As further adoption of hydraulic turbines to produce electricity is pursued, several engineering challenges have emerged [5]. Hydraulic

turbines are conventionally designed for operation within normal operating limits. When operating outside these limits, i.e. within temporary operating limits, the operating time is limited according to IEC 60609 standard [6]. If a turbine is operating in temporary operating limits in such a regime that pressure drops below vapor pressure, cavitation can occur. Cavitation can cause erosion of turbine components, independent of other erosion causes. Another challenge arises in rivers with suspended sediments, where the flowing water carries solid particles, which can cause additional erosion, termed abrasion.

To improve turbine design with respect to erosion phenomena, or to predict erosion in existing turbine designs, computational fluid dynamics (CFD) simulations coupled with erosion models are often utilized. In the past, various modelling approaches for cavitating flow have been adopted, and several cavitation erosion models have been developed. Research in this field remains ongoing, with recent efforts focused on phenomenological models applied to a range of engineering applications. Leclercq et al. [7] developed a cavitation erosion model based on earlier work by Fortes-Patella et al. [8] in which all cavitation collapses are considered by projecting cavitation erosion potential from interior cells to the wall using a discrete formulation. Implemented in Code Saturne, this model was successfully applied to predict cavitation erosion on a NACA65012 hydrofoil. Schenke and van Terwisga [9] proposed a continuous formulation for the projection of cavitation potential to walls, while Melissaris et al. [10] later improved the model by considering energy focusing during cavity collapse. Using this improvement, they were able to predict more spatially focused cavitation erosion patterns in the case of a KCD-193 model propeller. Arabnejad et al. [11] further advanced modeling by considering two different mechanisms, both pressure waves and microjets, depending on the distance from the wall at which cavity collapse occurs. These complex models have been successfully used to predict erosion for various cases; however,

open questions remain regarding modeling assumptions, particularly the cavitation collapse driving pressure [12].

In addition to above presented complex models, simpler models have been developed and successfully applied to predict cavitation erosion in different hydraulic systems. These simpler models are often applied to complex geometries or cases in which change in geometry needs to be considered. Such was the study by Brunhart et al. [13], where it has been determined that for the cavitation erosion prediction within a diesel fuel pump, where dynamic mesh was adopted, good agreement with experiment was obtained using an erosion indicator based on the recorded maximum of the squared total time derivative of pressure. Santos et al. [14] used three erosion indicators to predict cavitation erosion in gasoline direct injection (GDi) injector, where again dynamic mesh was adopted in the simulation. For the prediction of cavitation erosion in Pelton turbine, Jošt et al. [15] adopted criteria previously proposed by Rossetti et al. [16], which relate material damage to presence of water vapor in contact with the wall, rapid reduction in volume of this water vapor and the volume fraction of air mixed with the water (and water vapor) in the observed region. Based on this approach, Jošt et al. [15] concluded that damage of the observed Pelton rotor blades is not the result of cavitation erosion as the collapses are too slow.

Erosion of material due to particles has long been a topic of investigation of a distinct branch of engineering research – tribology. It stems from early research of contact forces due to friction by physicists such as Coulomb and later Hertz. Due to previously mentioned industry applications in which multiphase flows and subsequent abrasion occur, research into particle abrasion focused on experimental studies to obtain empirical predictive models of abrasion.

Such early study was conducted by Finnie [17], in which basic parameters that influence abrasion were determined, notably the influence of the particle impact angle on abrasion. Similarly, Bitter [18,19] identified different influencing parameters and proposed an empirical abrasion model, following by Grant and Tabakoff conducted studies [20,21] of abrasion in helicopter turbines and proposed a particle wall rebound model alongside their own abrasion model. Ahlert [22] proposed another abrasion model based on experimental investigation of particles impacting AISI 1018 steel sample. For AISI 4130 steel Forder et al. [23] conducted similar study and applied the abrasion model to predict abrasion in control valve using CFD simulations. Later multiple models have been proposed, with increasing complexity with respect to number of parameters considered, such as studies by Oka et al. [24] and Oka and Yoshida [25] and by Det Norske Veritas society (DNV) [26]. Over time adoption of empirical abrasion models in CFD has increased, Gnanavelu et al. [27] used this approach to reduce the number of experiments needed in their study of abrasion.

These empirical abrasion models have been applied to predict particle abrasion in different hydraulic systems by using CFD simulations of flows containing solid particles, where particles are considered as points and are tracked in Lagrangian frame. Peng and Cao [28] studied abrasion of pipe bends in piping found in oil industry, by comparing multiple abrasion models used in numerical simulations with experimental results, they concluded that McLaury model [29] in conjunction with the Grant and Tabakoff particle-wall rebound model [20,21] was the most accurate in predicting abrasion due to particles in liquid flow. Messa et al. [30] conducted a numerical study of abrasion in Pelton turbine injectors, where they applied the model by Oka et al. [24] and Oka and Yoshida [25] to predict abrasion of the nozzle seat and needle for different needle openings and needle vertex angles. They found enhanced abrasion for low openings and lower needle vertex angles. Many similar analyzes exist in the

literature, indicating the need to better understand abrasion of Pelton injectors, particularly for full scale Pelton turbine injectors, which has recently been analyzed by Liu et al. [31].

In general, abrasion of turbine components is prevalent also on turbine runners, specifically rotor blades. Kumar and Bhingole [32] conducted a CFD study of a combined effect of cavitation and particle erosion on Kaplan turbine, with varying particle size and concentration and determined that larger particles and larger concentrations of particles produced more abrasion on the runner. Similarly, effects of particle concentration and diameter on abrasion characteristics obtained by CFD simulations on a Pelton turbine runner have been studied by Li et al. [33], where they concluded that the diameter of the particles mainly effected the distribution of predicted abrasion regions and concentration mainly influenced the intensity of abrasion. Han et al. [34] also considered cavitation to have an influence on particle abrasion of Pelton runner, which they predicted using the Finnie [17] model. They concluded that cavitation has a clear influence on particle abrasion development, especially due to its effect on motion of smaller particles at the jet interface (airliquid interface) [34]. Table 1 summarizes the mechanisms of erosion and highlights the studies where erosion was modelled specifically in the case of Pelton runner.

Table 1. Summary of studies of erosion modelling highlighting which erosion mechanism was modelled

Mechanism of erosion
Cavitation collapse
Particle impact
Particle impact.
Particle impact and cavitation collapse
Particle impact
Particle impact

In the present study, we investigated numerically, whether the cause of erosion of Pelton runner, found in the previous study by Jošt et al. [15], could be due to solid particles present in the water flow. For this purpose, we extended the modelling of flow through Pelton turbine by including Lagrangian particle tracking and applying Finnie abrasion model within ANSYS CFX 2023 R2 [17]. Two particle concentrations were considered, one for regular river conditions and one for the case of heightened presence of particles, for example due to the extreme weather phenomena. Unlike previous studies, such as the one by Han et al. [34], we considered fully transient behavior of the flow including particle motion and Pelton rotor rotation. For this purpose, a sliding mesh approach was adopted, specifically a rotating mesh was used for the rotor region. With this approach we managed to avoid using a simplification to steady-state.

2 METHODS AND MATERIALS

2.1 Case Description

A Pelton runner from previous study is considered [15], where a numerical simulation of the existing prototype-scale Pelton turbine was conducted for the case of cavitating flow. The purpose of that study was to determine if cavitation could be the cause of erosion on the blade tip observed after prolonged operation as shown in Fig. 1.

The authors [15] concluded that cavitation alone could not explain the erosion in the region of the blade tip. The main question then arose, whether that damage could be the result of turbine operating in a river laden with sediments (solid particles).

The presence of sediment particles was confirmed by electron microscope imaging of the river water sample and both size and chemical composition of sediment particles were determined. Sediment particles were found to be in range between 30 μ m and 80 μ m and are visible on an electron microscope image shown in Fig. 2.

It was then found that sand particles, which are agglomerated to form a sediment particle, are silica particles (SiO2). Chemical composition of sediment for a wider sampling region Spectrum 1 and a sampling point Spectrum 2 (elongated particle visible in Fig. 2) is shown in Table 2, where Oxygen (O) and Silicone (Si) have the highest fraction of all elements present in sediment sample for both sampling regions Spectrum 1 and Spectrum 2.

Table 2. Chemical composition of sediment

Element	Spectrum 1	Spectrum 2	Element	Spectrum 1	Spectrum 2
0	45.43	48.21	K	2.42	0.58
С	13.68	16.17	Mg	0.87	-
Si	17.12	28.55	Na	0.54	0.44
Al	6.32	0.83	CI	-	0.11
Ca	9.29	3.42	Ti	0.33	0.18
Fe	3.67	1.51	Mn	0.32	-
			Total	100	100

2.2 Mathematical Model

An incompressible, turbulent, multiphase flow of water jet with cavitation and solid particles is considered. Multiphase flow of liquid water and due to cavitation water vapor contained within a jet, which forms an interface with respect to surrounding gas (air), is modelled using a homogeneous mixture approach. Mixture density (ρ) and mixture viscosity (μ) are determined by mixing rule as:

$$\rho = \varphi_l \rho_l + \varphi_v \rho_v + \varphi_g \rho_g, \tag{1}$$

$$\mu = \varphi_l \mu_l + \varphi_v \mu_v + \varphi_g \mu_g, \tag{2}$$

where φ_l is liquid volume fraction, φ_v is the vapor volume fraction and φ_g is gas volume fraction. Similarly, ρ_l and ρ_v are liquid and





Fig. 1. Damage of a Pelton rotor blade tip (in red bracket) after prolonged operation: a) view of the back side of the blade, view of the front side of the blade

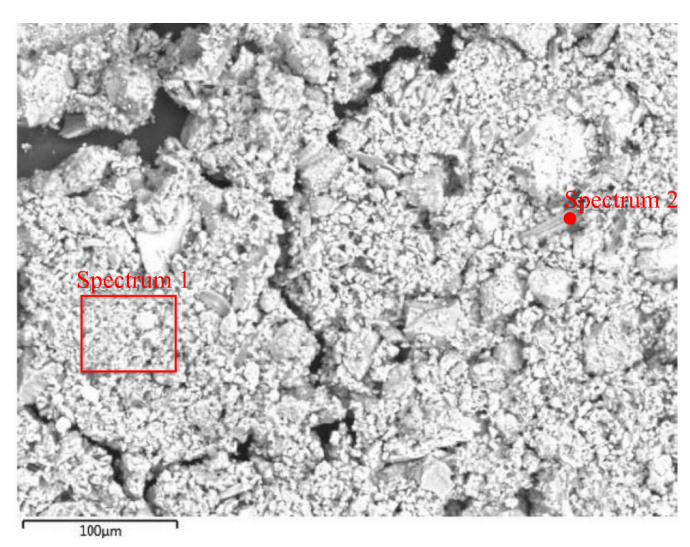


Fig. 2. Electron microscope image of the river sediment with two sampling positions to determine chemical composition indicated as Spectrum 1 and Spectrum 2

vapor density respectively and ρ_g is gas density. Finally, μ_l and μ_v are liquid and vapor dynamic viscosity respectively, while μ_g is gas dynamic viscosity. The governing equations of cavitating flow can then be written, the continuity equation as:

$$\frac{\partial \rho}{\partial t} + \nabla \left(\rho \mathbf{u} \right) = 0, \tag{3}$$

and momentum equation as:

$$\frac{\partial(\rho \mathbf{u})}{\partial t} + \nabla(\rho \mathbf{u} \mathbf{u}) = -\nabla p + \nabla \tau + \mathbf{S}_{\mathbf{M}}, \tag{4}$$

where Eqs. (3) and (4) are written for the mixture of liquid and vapor phases which share the same velocity $\bf u$ and pressure p. In Eq. (4) τ is mixture shear stress tensor and $\bf S_M$ is the momentum source term accounting for the presence of particles. Since the multiphase flow is considered as a mixture of two phases, an additional equation for transport of vapor volume is needed:

$$\frac{\partial \varphi_{v}}{\partial t} + \nabla \left(\varphi_{v} \mathbf{u} \right) = \frac{\dot{m}}{\rho_{l}},\tag{5}$$

where \dot{m} is the interface mass transfer rate due to cavitation, for which a cavitation model by Zwart et al. [35] was adopted in this study:

$$\dot{m} = \begin{cases} -F_e \frac{3r_{muc} (1 - \varphi_v) \rho_v}{R_B} \sqrt{\frac{2}{3} \frac{p_v - p}{\rho_l}}, & \text{if } p < p_v \\ F_c \frac{3\varphi_v \rho_v}{R_B} \sqrt{\frac{2}{3} \frac{p - p_v}{\rho_l}}, & \text{if } p > p_v \end{cases}$$
(6)

where F_e is the evaporation coefficient with a recommended value of 50 [35], F_c is the condensation coefficient with a recommended value of 0.01, r_{nuc} is the nucleation site volume fraction with a default value of 5×10^{-4} and R_B is the bubble radius upon which the model is derived, with a recommended value of 10^{-6} m [35]. From Eq. (6) it is evident that the mass transfer rate was considered negative in the case of evaporation, when pressure p is bellow vapor pressure p_v , which was 1300 Pa for water. Likewise, in Eq. (6) the mass transfer rate is positive in the case of condensation, when the pressure p is above vapor pressure p_v .

Although more advanced turbulence models (hybrid Reynolds-averaged Navier-Stokes and large Eddy simulation (RANS/LES), and large Eddy simulation (LES)) have recently been used in the studies of turbulent, cavitating flows [36], even for some engineering applications [37,38], RANS two-equation models still represent a good balance between accuracy and calculation times for most engineering applications, like a Pelton turbine. Therefore, in this study turbulence was modelled using a RANS approach, specifically the $k-\omega$ SST two-equation turbulence model was used. Two additional transport equation are introduced, one for the turbulent kinetic energy k:

$$\frac{\partial(\rho k)}{\partial t} + \nabla(\rho k \mathbf{u}) = \nabla \left[\left(\mu + \frac{\mu_t}{\sigma_k} \right) \nabla k \right] + G_k - Y_k + S_k, \tag{7}$$

and one for the specific turbulence dissipation rate ω :

$$\frac{\partial(\rho\omega)}{\partial t} + \nabla(\rho\omega\mathbf{u}) = \nabla\left[\left(\mu + \frac{\mu_t}{\sigma_\omega}\right)\nabla\omega\right] + G_\omega - Y_\omega + D_\omega + S_\omega, \quad (8)$$

where G_k and G_ω are production terms for the turbulent kinetic energy and the specific turbulence dissipation rate respectively, Y_k and Y_ω are the dissipation terms for the turbulent kinetic energy and for the specific turbulence dissipation rate respectively, σ_k and σ_ω are the turbulent Prandtl numbers for k and for ω respectively, S_k and S_ω are the source terms. Since the $k-\omega$ scale-adaptive simulation model (SST) is a blended turbulence model, consisting of standard $k-\varepsilon$ and standard $k-\omega$ model, an additional term cross-diffusion term D_ω is introduced in Eq. (8) due to reformulation of $k-\varepsilon$ model for blending with $k-\omega$ model. RANS approach results in additional turbulent viscosity μ_l , which is in the case of $k-\omega$ SST model written as:

$$\mu_{t} = \frac{\rho k}{\omega} \frac{1}{\max \left[\frac{1}{\alpha^{*}}, \frac{SF_{2}}{a_{1}\omega} \right]},\tag{9}$$

where α^* is the turbulent viscosity damping coefficient, a_1 is a model constant with value of 0.31 [39], S is the strain rate magnitude and F_2 is the second blending function. A detailed description of the turbulent model used is available in [39].

Particles represent a discrete phase for which Lagrangian tracking is adopted within previously described continuous phase (mixture of two continuous phases) which was considered in Eulerian frame. In our study drag force and virtual mass force were considered, gravity effects (buoyancy) were neglected as the inertia of the flow, due to high fluid velocity, had a dominant influence on the motion of particles. Then, an additional motion equation for particles due

to drag force and virtual mass force can be written in the form of particle acceleration as:

$$\frac{d\mathbf{v}}{dt} = \frac{18\mu_l}{\rho_p d_p^2} \frac{C_D R e_p}{24} (\mathbf{u} - \mathbf{v}) + \frac{1}{2} \frac{\rho_l}{\rho_p} \left(\frac{D\mathbf{u}}{Dt} - \frac{d\mathbf{v}}{dt} \right), \tag{10}$$

where \mathbf{v} is the particle velocity, ρ_{v} is the particle density, d_{p} is the particle diameter and the particle Reynolds number Re_{p} is defined as:

$$Re_{p} = \frac{\rho_{p} d_{p} |\mathbf{u} - \mathbf{v}|}{\mu_{t}},\tag{11}$$

The drag coefficient C_D is calculated using the Schiller Naumann correlation [40]:

$$C_{D} = \begin{cases} 24 \frac{\left(1 + 0.15Re_{p}^{0.687}\right)}{Re_{p}}, & \text{if } Re_{p} < 1000\\ 0.44, & \text{if } Re_{p} \ge 1000 \end{cases}$$
 (12)

Since the volume fraction of the particles in particle-laden flow is low, interactions between particles are neglected. However, interaction of particles with the wall must be considered as it is one of the boundary conditions. For this, Hard Sphere Model is adopted, where particles are considered as nondeformable during their collision with the wall. Rebound of particles from the wall is then described with two coefficients of restitution, one in wall normal direction:

$$e_n = \frac{v_{n,2}}{v_{n,1}},\tag{13}$$

and one in tangential direction:

$$e_{t} = \frac{v_{t,2}}{v_{t,1}},\tag{14}$$

where $v_{n,1}$ and $v_{n,2}$ are particle velocities in the wall normal direction before and after rebound respectively, and $v_{t,1}$ and $v_{t,2}$ are particle velocities in the wall tangential direction before and after rebound respectively. Particle velocity in both directions after rebound $(v_{n,2}$ and $v_{t,2})$ are calculated for the known coefficients of restitution $(e_n$ and $e_t)$, which were determined by using Grant and Tabakoff model [19], where coefficients of restitution are given as functions of particle impact angle γ as:

$$e_n = 0.993 - 1.76\gamma + 1.56\gamma^2 - 0.49\gamma^3, \tag{15}$$

$$e_t = 0.988 - 1.76\gamma + 1.56\gamma^2 - 0.49\gamma^3. \tag{16}$$

To predict erosion of the wall due to impacting particles, we used an empirical model by Finnie [17], which gives the erosion rate as:

$$E_{R} = \left(\frac{|\mathbf{v}|}{v_{0}}\right)^{n} f(\gamma), \tag{17}$$

where v_0 is the empirical reference velocity with a value of 3321 m/s for steel, n is the velocity exponent with a value of 2.4 and $f(\gamma)$ is an impact angle function, given as:

$$f(\gamma) = \begin{cases} \frac{1}{3}\cos^2\gamma; & \text{if } \tan\gamma > \frac{1}{3} \\ \sin(2\gamma) - 3\sin^2\gamma, & \text{if } \tan\gamma \le \frac{1}{3} \end{cases}$$
 (18)

2.3 Boundary Conditions and Physical Properties

Based on the previously described sediment analyzis, solid silica particles with density ρ_p =2650 kg/m³ of sizes between 30 µm and 80 µm were considered in numerical simulation. To account for the varying size of particles we used the Rosin-Rammler particle size distribution, where the mass fraction of particles above a certain particle diameter d_p is defined as:

$$R = e^{\left[-\left(\frac{d_p}{d_e}\right)^2\right]},\tag{19}$$

where d_e is the size constant and χ is the size distribution parameter. We considered a particle distribution with d_e =50 μ m and χ =1.1. The resulting cumulative mass fraction distribution is shown in Fig. 3.

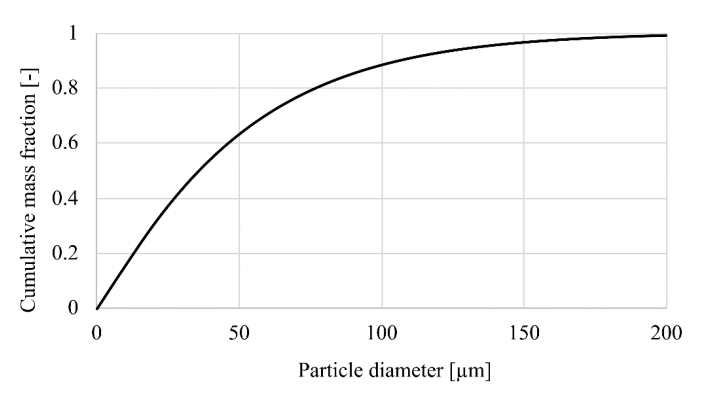


Fig. 3. Rosin-Rammler particle size distribution used in numerical simulation, represented with a cumulative mass fraction over particle diameters

Varying shape of particles was not considered in numerical simulations; therefore, particles were assumed to be spherical. Two different cases of particle loading of the flow were considered, one for the regular river flow where volume fraction of particles is 0.006 % and one for heightened particle loading scenario where volume fraction of particles is 10 times higher, resulting in volume fraction of particles of 0.06 %. Properties of liquid water, water vapor and air are presented in Table 3.

Table 3. Properties of continuous phases (liquid water, water vapor and air) used in numerical simulation

Material	Density [kg/m³]	Dynamic viscosity [Pa s]
Liquid water	999.18	0.00114029
Water vapor	0.02308	9.86e-6
Air	1.185	1.83e-5

Boundary conditions were defined as shown in Fig. 4. For the liquid jet flow, velocity components were prescribed as a function of coordinates over the nozzle area, which were determined with previous numerical simulation of flow through the injector [15] for the mean velocity magnitude of 105.233 m/s and 5 % turbulent intensity at the inlet. For the particles entering the domain with the jet, zero-slip velocity condition was used while injection of particles

was realized by prescribing their number rate and mass flow rate. This is presented in Table 4 for both particle loading scenarios.

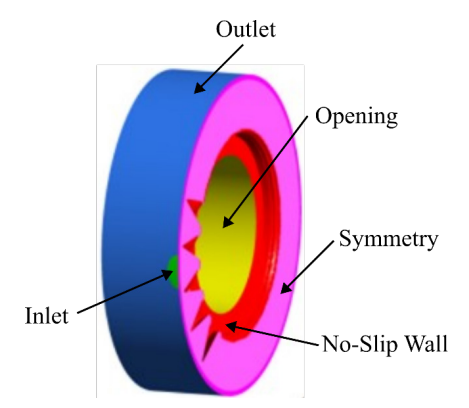


Fig. 4. Boundary conditions marked by colors: green – inlet, blue – outlet, red – no-slip wall, purple – symmetry and yellow – opening

Table 4. Particle injection definition at the inlet

Particle loading scenario	Volume fraction [%]	Number rate [s ⁻¹]	Mass flow rate [kg/s]
Normal	0.006	2.81794e+7	0.048875
Heavy	0.06	2.81794e+8	0.48875

At the outlet, static pressure was prescribed with a value of 101,300 Pa for continuous phase, and particles are given the escape boundary condition by default. Same conditions were prescribed for the opening boundary condition.

To reduce computational demands, symmetry boundary condition was used at symmetry plane as shown in Fig. 4. For particles, however, this symmetry plane represented a wall, the fact that only half of the full volume (domain) was considered was accounted for when calculating particle inlet number rate and mass flow rate presented in Table 4.

Remaining surfaces (rotor blades and hub) were treated as noslip walls for the continuous phase and solid walls with a rebound boundary condition for particles.

2.4 Mesh and Numerical Setup

To further reduce the computational demands, we considered only 5 rotor blades in the geometrical model for the meshing, since mesh around the blades require refinement resulting in higher mesh cell density. We used the mesh from the previous study [15], where a mixed hexahedral and tetrahedral mesh with 10.75 million cells was used. The mesh is presented in Fig. 5. The mesh consisted of two main regions, stationary and rotating. Rotating region of mesh

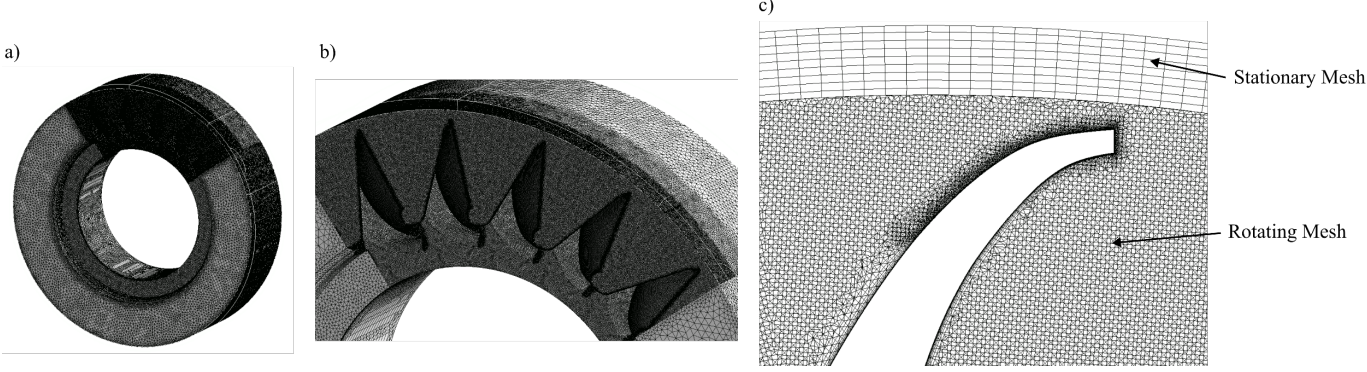


Fig. 5. Mesh showing: a) full mesh, b) detailed view of the blade region on the symmetry plane, and c) detailed view around a single blade at cross-section

was prescribed mesh rotation, such that 0.1° of rotor rotation was achieved per time step, and in total 27° of rotor rotation was achieved during the simulation.

Since the simulation was fully transient, a second order backward Euler transient scheme was adopted and for the advection terms high resolution scheme was used. Within each time step maximum 10 iterations were performed, however a residual target of 1e-4 was achieved before this limit.

3 RESULTS AND DISCUSSION

First, we present the results for the flow of sand particles in water jet impacting Pelton rotor blades, which is shown in Fig. 6 for the normal particle loading scenario and in Fig. 7 for the heavy particle loading scenario. In Figs. 6 and 7 we observe jet (green) impacting Pelton rotor blades shown at different times, with visible cavitation (magenta) shown as iso-surface with 20 % volume fraction of vapor and sand particles (black) for a normal particle loading scenario and heavy particle loading scenario, respectively. Rotor blade on which subsequent erosion is studied is highlighted with orange color. At the beginning in a) the blade is yet to come in contact with the jet, in following moments b) through e) it passes through the jet, particles in the jet impact the blade and in f) finally jet is cut-off by next passing blade

The difference in particle loading is clearly shown and discernible when comparing Figs. 6 and 7. Due to the modelling approach taken in this work, jet development and cavitation development are not influenced by particles, therefore they are identical for both particle loadings, as seen when comparing Figs. 6 and 7.

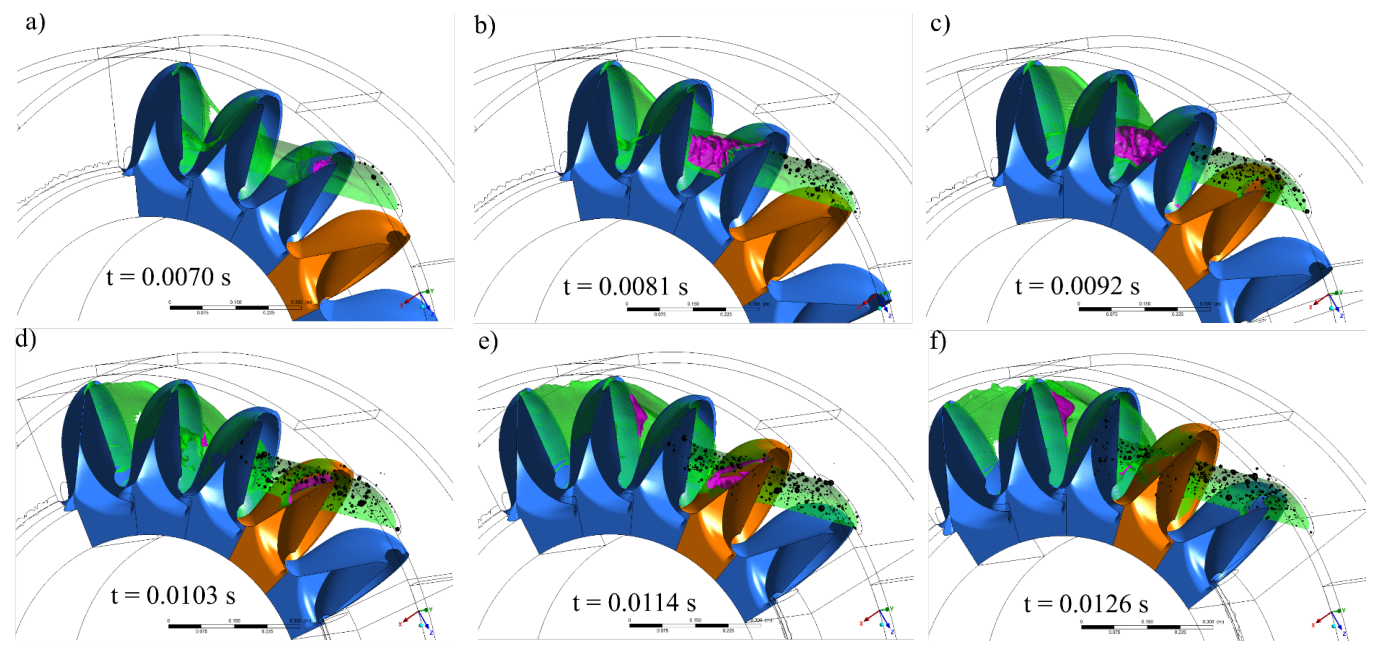


Fig. 6. Impact of jet with particles on Pelton rotor blade at different times for normal particle loading scenario

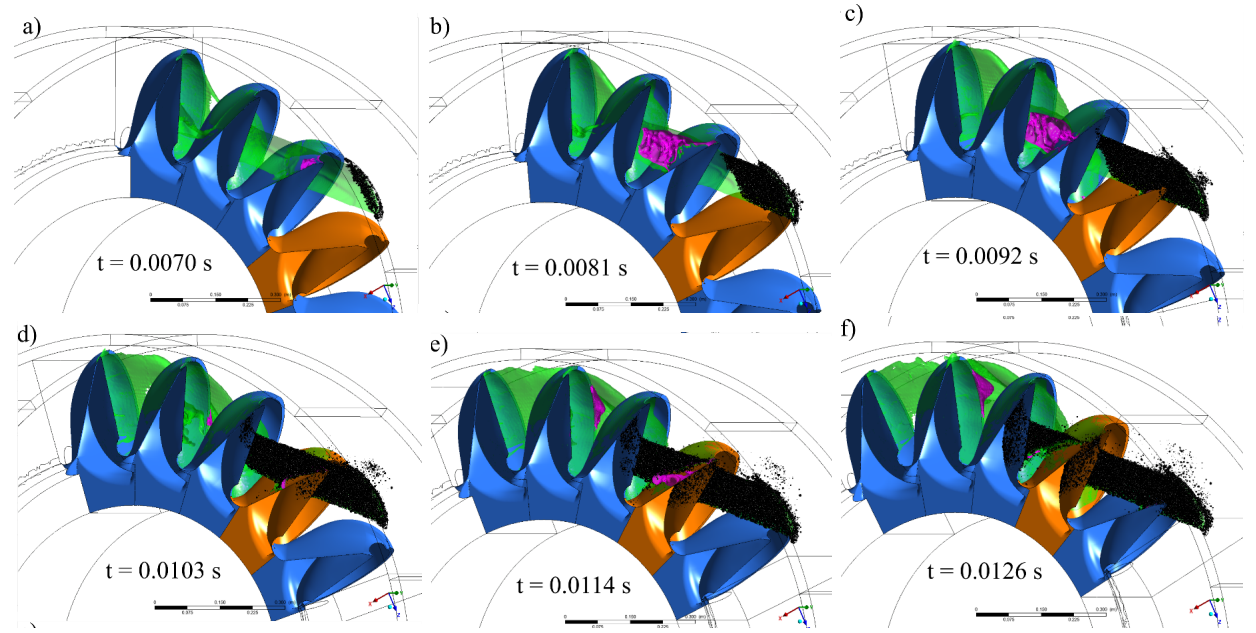


Fig. 7. Impact of jet with particles on Pelton rotor blade at different times for heavy particle loading scenario

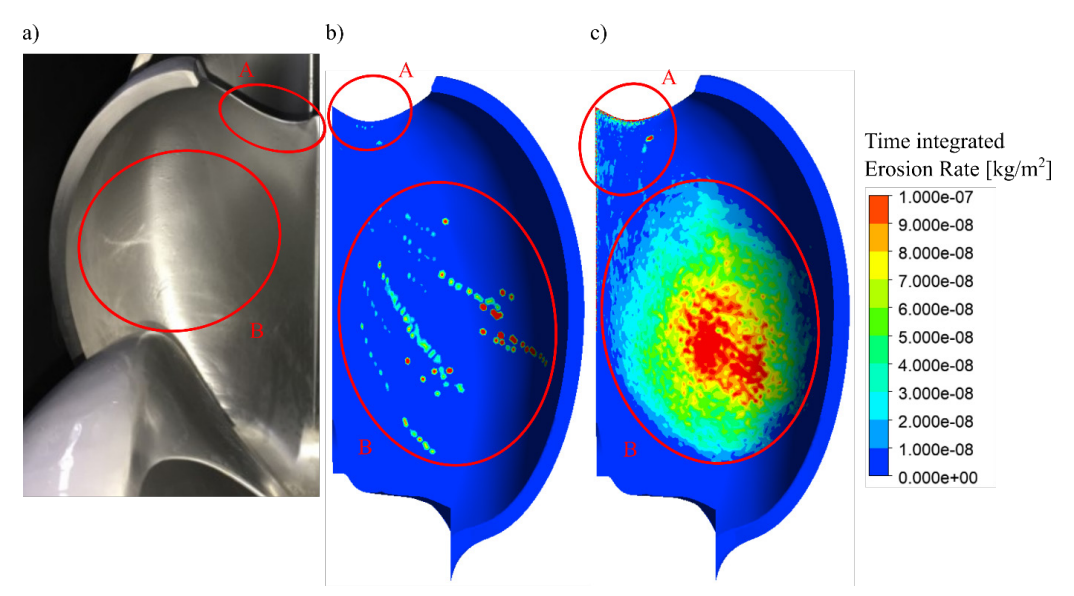


Fig. 8. Erosion on the front side of the Pelton rotor blade: a) real operating blade, b) normal particle loading scenario simulation, and c) heavy particle loading scenario simulation

Particle motion follows the motion of the water jet. Attached cavitation pocket behind the second blade, visible at time t = 0.0114 s on Figs. 6 and 7, redirects the particles around it. Within the simulated time, the second blade of five blades considered in this simulation passes through the impacting water jet carrying sand particles completely. As the second blade passes through the jet, particles entrained in the jet impact the back side of the blade as well.

This is why erosion prediction results will be presented only for the second blade, since particle erosion is expected to occur on both the front and the back side of the blade. Particle erosion on the front side of the blade is shown in Fig. 8, where contour of time integral of Eq. (17) is shown for both particle loading scenarios. Two distinct erosion zones are marked as A – blade tip region, and B – blade bucket. Difference in the pattern of zone B is observed, for heavier particle loading case (Fig. 8c) a more spread-out pattern emerges.

Presented simulation results show that the extent of abrasion is higher in the heavy particle loading case, while in both normal and heavy loading scenarios two distinct erosion zones are formed on the front side of the blade. One is at the tip of the blade and is more pronounced in the heavy particle loading scenario. Second one is in the middle of the blade bucket and is again more pronounced in the heavy particle loading scenario. The difference between the erosion zone B pattern in Fig. 8 can be explained by larger number of particles in the flow in the heavy particle loading scenario. Due to larger number of particles, which take up more configurations in space (in the water jet), they produce a more spread-out pattern. These results of erosion patterns for the front side of the blade are also in general agreement with reference lab-scale experimental investigation of Pelton bucket by Umar et al. [41], where they also observed two distinct erosion zones (one around the blade splitter and one in the middle of the bucket). Direct comparison is however limited, by different Pelton geometry, operating parameters and sediment concentration.

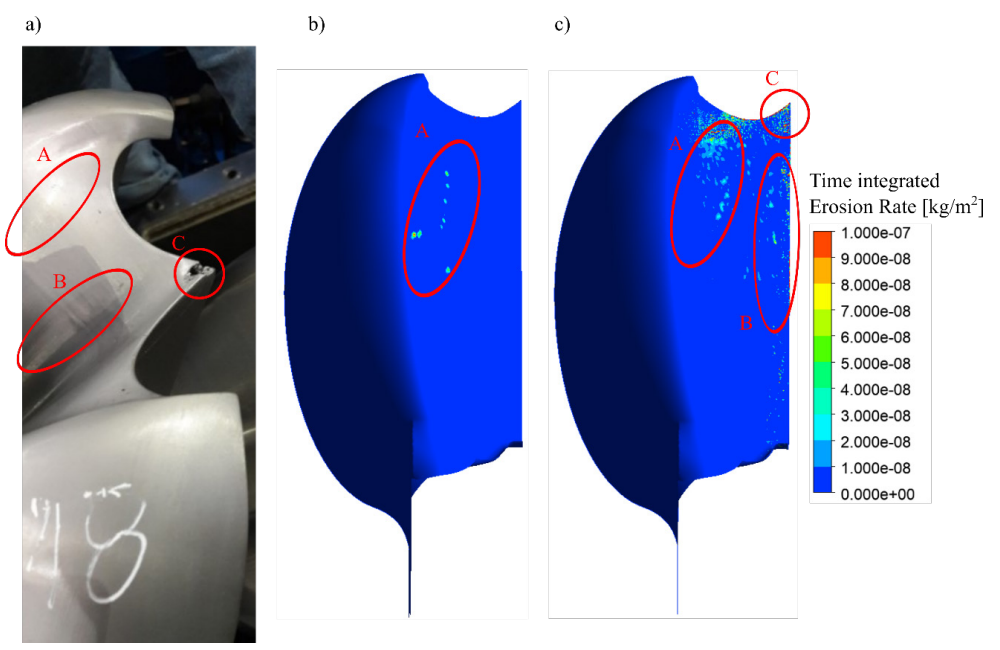


Fig. 9. Erosion on the back side of the Pelton rotor blade: a) real operating blade, b) normal particle loading scenario simulation, c) heavy particle loading scenario simulation

Similarly, we present erosion on the back side of the blade in Fig. 9. Three distinct erosion zones are marked as A- blade mid-bucket region, B- blade bucket edge, and C- blade tip region. On the blade of real operating Pelton rotor, three erosion zones can be identified, (Fig. 9a), one in the middle of the bucket, one at the edge, splitting the blade in two halves, and one around the blade tip. All three regions are observed in the case of the simulation with the heavy particle loading, however, for the normal particle loading condition only the region in the middle of the bucket (Fig. 9b) region marked with A is predicted. In general, it is observed that the extent of erosion is less on the back of the blade than on the front side.

Since from the previous study a research question was whether particles could be the cause of blade tip damage, a detailed view of the blade tip is shown in Fig. 10. Results of simulation with heavy particle loading only are shown in Fig. 10a), as in the normal particle loading no erosion of the tip was predicted (Fig. 9). Under normal particle loading of the river, tip damage observed after operation of a real Pelton rotor as seen in Fig. 10b), can't be attributed to particle erosion. However, under heavy loading conditions, particle erosion could cause damage to the tip, simulation results for these conditions show good agreement. Erosion rate is highest at the tip and the spreads out with lower intensity, and black lines in Fig. 10 indicate the extent of erosion spread.

Finally, we give brief discussion of model sensitivity to different parameters or modelling scenarios. Particles were assumed to be spherical, however real river sediment particles come in different shapes. An example of idealized non-spherical shape is a superellipsoid, for which Wedel et al. [42] found that Lagrangian tracking gives better particle motion than by using simpler shape factors, indicating the complexity of this problem. This difference in particle motion could then be reflected in the erosion pattern at the wall. The influence of particles on erosion could also be due to irregular shape of particles, for example angular particles are known to be more erosive. Yasser, Zhou and El- Emam [43] conducted detailed computational fluid dynamics - discrete element method (CFD-DEM) simulations of different angular particles and spherical particles in pipe elbow and found that particles with fewer corners (but therefore sharper edges) produced more erosion, while pattern of erosion was more localized. In addition to that, even for spherical particles different drag models exist. Likewise, there are several approaches to model cavitation and within the vapor transport equation modelling approach adopted in this study, several algebraic cavitation models exist. For an overview of different cavitation models, we refer the reader to Folden and Aschmoneit [44].

4 CONCLUSIONS

This study presents a numerical investigation into the erosion of Pelton turbine rotor due to solid particles in a cavitating flow. By extending previous research that focused on cavitation-induced erosion, we incorporated Lagrangian particle tracking and employed the Finnie abrasion model [17] to assess the effects of sediment-laden water on turbine blades. Our findings indicate that, under normal river conditions, particle-induced erosion is not a significant contributor to the observed blade tip damage but can cause erosion of the blade bucket. However, under heavy sediment loading scenario, as a result of extreme weather phenomena, erosion predictions closely align with real-world observation on an actual operating Pelton rotor, suggesting that heavy particle concentrations can lead to substantial material loss, particularly at the blade tip.

The results highlight the necessity of considering both cavitation and particle erosion when evaluating turbine durability in sediment-rich environments. Future work could focus on refining erosion models by incorporating particle shape effects, varying material properties, and exploring mitigation strategies such as optimized blade coatings or operational adjustments to minimize erosive wear.

Nomenclature

```
turbulent viscosity damping coefficient, [-]
     impact angle, [°]
γ
     size distribution parameter, [-]
χ
     liquid volume fraction, [-]
\varphi_I
     vapor volume fraction, [-]
\varphi_{v}
     gas volume fraction, [-]
μ
     mixture viscosity, [Pa s]
     liquid dynamic viscosity, [Pa s]
\mu_l
     vapor dynamic viscosity, [Pa s]
     gas dynamic viscosity, [Pa s]
     specific turbulence dissipation rate, [s<sup>-1</sup>]
ω
     mixture density, [kg/m<sup>3</sup>]
ρ
     liquid density, [kg/m<sup>3</sup>]
     gas density, [kg/m<sup>3</sup>]
```

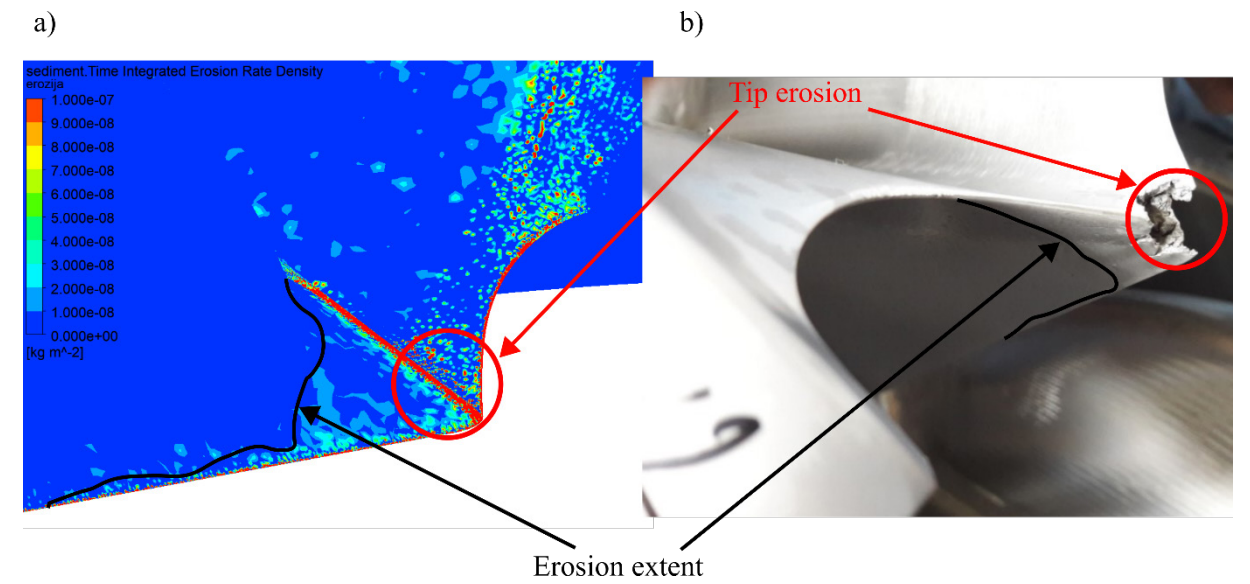


Fig. 10. Erosion of the tip of the blade: a) simulation for heavy particle loading condition, b) actual Pelton rotor blade tip

- ρ_p particle density, [kg/m³]
- ρ_{ν} vapor density, [kg/m³]
- σ_k turbulent Prandtl number for the turbulent kinetic energy, [-]
- σ_{ω} turbulent Prandtl number for the specific turbulence dissipation rate, [-]
- τ mixture shear stress tensor, [Pa]
- a_1 model constant, [-]
- C_D drag coefficient, [-]
- d_n particle diameter, [m]
- d_e size constant, [-]
- e_n coefficient of restitution in wall normal direction, [-]
- e_t coefficient of restitution in wall tangential direction, [-]
- F_{ρ} evaporation coefficient, [-]
- F_d condensation coefficient, [-]
- F_2 second blending function, [-]
- $f(\gamma)$ is an impact angle function, [-]
- G_k production term for the turbulent kinetic energy, [m²/s²]
- G_{ω} production term for the specific turbulence dissipation rate, $[\mathrm{m}^2/\mathrm{s}^3]$
- k turbulent kinetic energy, $[m^2/s^2]$
- \dot{m} interface mass transfer rate, [kg/s]
- *n* velocity exponent, [-]
- p pressure, [Pa]
- p_{ν} vapor pressure, [Pa]
- R mass fraction of particles, [-]
- R_B bubble radius, [m]
- *Re_p* particle Reynolds number, [-]
- S strain rate magnitude, [s⁻¹]
- S_{M} momentum source term, [N
- S_k source term for the turbulent kinetic energy, [m²/s²]
- S_{ω} source term for the specific turbulence dissipation rate, [m²/s³]
- t time, [s]
- u velocity, [m/s]
- v particle velocity, [m/s]
- v_n particle velocity in the wall normal direction, [m/s]
- v_t particle velocity in the wall tangential direction, [m/s]
- v_0 empirical reference velocity, [m/s]
- Y_k dissipation term for the turbulent kinetic energy, [m²/s²]
- Y_{ω} dissipation term for the specific turbulence dissipation rate, $[m^2/s^3]$

References

- Vovk, N., Ravnik, J. Numerical modeling of two-phase flow inside a wet flue gas absorber sump. Energies 16 8123 (2023) D0I:10.3390/en16248123.
- [2] Gautam S., Acharya, N., Lama, R., Chitrakar, S., Neopane, H.P. Zhu, B., Dahlhaug, O.G. Numerical and experimental investigation of erosive wear in Francis runner blade optimized for sediment laden hydropower projects in Nepal Sust. Ener Tech Assess 51 101954 (2022) D0I:10.1016/j.seta.2022.101954.
- [3] IEA. SDG7: Data and Projections (2024) https://www.iea.org/reports/sdg7-dataand-projections, accessed 2025-09-22.
- [4] Kent, R. Renewables. *Plast Eng* 74 56-57 (2018) **D0I:10.1002/peng.20026**.
- [5] Giljen, Z., Nedeljković, M., Cheng, Y. The influence of pump-turbine specific speed on hydraulic transient processes. Stroj vest-J Mech E 70 231-246 (2024) D0I:10.5545/sv-jme.2023.776.
- [6] CEI/IEC 60609-1:2004 Hydraulic Turbines, Storage Pumps and Pump-Turbines -Cavitation Pitting Evaluation -Part 1: Evaluation in Reaction Turbines, Storage Pumps and Pump-Turbines. International Organization for Standardization, Geneva
- [7] Leclercq, C., Archer, A., Fortes-Patella, R., Cerru, F. Numerical cavitation intensity on a hydrofoil for 3D homogeneous unsteady viscous flows. Int J Fluid Mach Syst 10 254-263 (2017) D0I:10.5293/IJFMS.2017.10.3.254.
- [8] Fortes Patella, R., Reboud, J.-L., Briancon Marjollet, L. A phenomenological and numerical model for scaling the flow agressiveness in cavitation erosion. EROCAV Workshop (2004) https://www.researchgate.net/publication/281921326, accessed 2025-09-22.
- [9] Schenke, S., van Terwisga, T.J.C. An energy conservative method to predict the erosive aggressiveness of collapsing cavitating structures and cavitating flows from numerical simulations. Int J Multiph Flow 111 200-218 (2019) D0I:10.1016/j.ijmultiphaseflow.2018.11.016.

- [10] Melissaris, T., Schenke, S., Bulten, N., van Terwisga, T.J.C. On the accuracy of predicting cavitation impact loads on marine propellers. Wear 456-457 203393 (2020) D0I:10.1016/i.wear.2020.203393.
- [11] Arabnejad, M.H., Svennberg, U., Bensow, R.E. (2021). Numerical assessment of cavitation erosion risk using incompressible simulation of cavitating flows. Wear 464-465 203529 (2021) DOI:10.1016/j.wear.2020.203529.
- [12] Kevorkijan, L., Pezdevšek, M., Biluš, I., Hren, G. Cavitation erosion modelling comparison of different driving pressure approaches. *In. J Simul Model* 22 233-244 (2023) D0I:10.2507/IJSIMM22-2-639.
- [13] Brunhart, M., Soteriou, C., Daveau, C., Gavaises, M., Koukouvinis, P., Winterbourn, M. Cavitation erosion risk indicators for a thin gap within a diesel fuel pump. Wear 442-443 203024 (2020) D0I:10.1016/j.wear.2019.203024.
- [14] Gomez Santos, E., Shi, J., Venkatasubramanian, R., Hoffmann, G., Gavaises, M., Bauer, W. Modelling and prediction of cavitation erosion in GDi injectors operated with E100 fuel. Fuel 289 119923 (2021) D0I:10.1016/j.fuel.2020.119923.
- [15] Jošt, D., Škerlavaj, A., Pirnat, V., Morgut, M. Nobile, E. Detailed analyzis of flow in two pelton turbines with efficiency and cavitation prediction. *Int J Fluid Mach Syst* 12 388-399 (2019) D0I:10.5293/IJFMS.2019.12.4.388.
- [16] Rossetti, A., Pavesi, G., Ardizzon, G., Santolin, A. Numerical analyzes of cavitating flow in a Pelton turbine. J Fluid Eng-T ASME 136 081304 (2014) D0I:10.1115/1.4027139.
- [17] Finnie, I. Erosion of surfaces. Wear 3 87-103 (1960) D0I:10.1016/0043-1648(60)90055-7.
- [18] Bitter, J.G.A. A study of erosion phenomena: Part I. Wear 6 5-21 (1963) D0I:10.1016/0043-1648(63)90003-6.
- [19] Bitter, J.G.A. A study of erosion phenomena: Part II. Wear 6 169-190 (1963) D0I:10.1016/0043-1648(63)90073-5.
- [20] Grant, G., Tabakoff, W. Erosion prediction in turbomachinery resulting from environmental solid particles J Aircraft 12 471-478 (1975) D0I:10.2514/3.59826.
- [21] Grant, G., Tabakoff, W. An Experimental Investigation of the Erosive Characteristics of 2024 Aluminum Alloy. NTIS, Springfield (1973).
- [22] Ahlert, K.R. Effects of Particle Impingement Angle and Surface Waiting on Solid particle Erosion of AISI 1018 Steel. MScThesis (1994) University of Tulsa, Tulsa.
- [23] Forder, A., Thew, M., Harrison, D. A numerical investigation of solid particle erosion experienced within oilfield control valves. Wear 216 184-193 (1998) D0I:10.1016/S0043-1648(97)00217-2.
- [24] Oka, Y.I., Okamura, K. Yoshida, T. Practical estimation of erosion damage caused by solid particle impact: Part 1: Effects of impact parameters on a predictive equation. Wear 259 95-101 (2005) DOI:10.1016/j.wear.2005.01.039.
- [25] Oka, Y.I., Yoshida, T. Practical estimation of erosion damage caused by solid particle impact: Part 2: Mechanical properties of materials directly associated with erosion damage. Wear 259 102-109 (2005) D0I:10.1016/j.wear.2005.01.040.
- [26] Det Norske Veritas. Erosive Wear in Piping Systems. https://rules.dnv.com/docs/pdf/dnvpm/codes/docs/2015-08/RP-0501.pdf, accessed on 2025-09-22
- [27] Gnanavelu, A., Kapur, N., Neville, A., Flores, J.F., Ghorbani, N. A numerical investigation of a geometry independent integrated method to predict erosion rates in slurry erosion. Wear 271 5-6 712-719 (2011) D0I:10.1016/j. wear.2010.12.040.
- [28] Peng, W., Cao, X. Numerical simulation of solid particle erosion in pipe bends for liquid-solid flow. *Powder Technol* 294 266-279 (2016) D0I:10.1016/j. powtec.2016.02.030.
- [29] McLaury, B.S., Shirazi, S.A., Shadley, J.R., Rybicki, E.F. Modeling erosion in chokes. Proceedings of ASME Fluids Eng. (1996) 773-782.
- [30] Messa, G.V., Mandelli, S., Malavasi, S. Hydro-abrasive erosion in Pelton turbine injectors: A numerical study. Renew Energ 130 474-488 (2019) D0I:10.1016/j. renene.2018.06.064.
- [31] Liu, J., Pang, J. Liu, X., Huang, Y., Deng, H. Analysis of sediment and water flow and erosion characteristics of large Pelton turbine injector. *Processes* 11 1011 (2023) D0I:10.3390/pr11041011.
- [32] Kumar, D., Bhingole, P.P. CFD based analysis of combined effect of cavitation and silt erosion on Kaplan turbine. *Mater Today-Proc* 2 2314-2322 (2015) D0I:10.1016/j.matpr.2015.07.276.
- [33] Li, L., Lu, J., Gong, Y., Zhao, H., Liu, X., Zhu, B. Sediment erosion characteristics of Pelton turbine runner: Effects of sediment concentration and diameter. *Renew Energ* 220 119679 (2024) D0I:10.1016/j.renene.2023.119679.
- [34] Han, L., Guo, C., Yuan, Y., Li, D., Liu, Y., Iranzo, A., Qin, D. Investigation on sediment erosion in bucket region of Pelton turbine considering cavitation. *Phys Fluids* 36 023305 (2024) D0I:10.1063/5.0179387.
- [35] Zwart, P.J., Gerber, A.G. Belamri, T. A two-phase flow model for predicting cavitation dynamics. Proceedings of International Conference on Multiphase Flow 152 (2004).

- [36] Decaix, J., Goncalvès, E. Investigation of three-dimensional effects on a cavitating Venturi flow. Int J Heat Fluid FI 44 576-595 (2013) D0I:10.1016/j. ijheatfluidflow.2013.08.013.
- [37] Drešar, P. Development of Biofluid Pump. PhD Thesis University of Ljubljana, Ljubljana (2020). (in Slovene)
- [38] Zhang, X. Transient flow characteristics of a pressure differential valve with different valve spool damping orifice structures. Stroj vestn-J Eng E 70 141-158 (2024) D0I:10.5545/sv-jme.2023.691.
- [39] Menter, F.R. Two-equation eddy-viscosity turbulence models for engineering applications. *AIAA J* 32 1598-1605 (1994) **D0I:10.2514/3.12149**.
- [40] Schiller, L., Naumann, A. A Drag Coefficient Correlation. Z Ver Dtsch Ing 77 318-320 (1935).
- [41] Umar, B.M., Wang, Z., Chitrakar, S., Thapa, B., Huang, X., Poudel, R., Karna, A. Experimental erosion flow pattern study of Pelton runner buckets using a non-recirculating test rig. Energies 17 4006 (2024) DOI:10.3390/en17164006.
- [42] Wedel, J., Steinmann, P., Štrakl, M., Hriberšek, M., Ravnik, J. Shape matters: Lagrangian tracking of complex nonspherical microparticles in superellipsoidal approximation. Int J Multiphase Flow 158 104283 (2023) D0I:10.1016/j. ijmultiphaseflow.2022.104283.
- [43] Yasser, E., Zhou, L., El-Emam, M.A. Numerical analysis of particle shape influence on erosion and flow behavior in a 90-degree elbow pipe under Solid-Liquid flow. Adv Powder Technol 36 104928 (2025) D0I:10.1016/j.apt.2025.104928.
- [44] Folden, T.S., Aschmoneit, F.J. A classification and review of cavitation models with an emphasis on physical aspects of cavitation. *Phys Fluids* 35 081301 (2023) D0I:10.1063/5.0157926.

Acknowledgements The authors wish to thank dr. Dragica Jošt for her assistance in the transfer and explanation of the previous case, as well as her kind openness for discussion. Additionally, we thank the Slovenian Research Agency (ARRS) for its financial support in the framework of Research Program P2-0196 in Power, Process, and Environmental Engineering.

Received: 2025-04-16, revised: 2025-07-13, accepted: 2025-07-24 as Original Scientific Paper 1.01.

Data Availability The data that support the findings of this study are not available due to project confidentiality.

Author Contribution Luka Kevorkijan: Formal Analysis, Investigation, Writing – original draft, Software, Visualization; Matjaž Hriberšek: Conceptualization, Methodology, Project Administration, Supervision; Luka Lešnik: Investigation, Writing – review & editing, Visualization; Aljaž Škerlavaj: Conceptualization, Data curation, Methodology, Validation; Ignacijo Biluš: Investigation, Supervision, Writing- original draft, Writing – review & editing.

Numerična raziskava erozije zaradi delcev v kavitirajočem toku skozi Peltonovo turbino

Pozetek Erozija komponent Peltonove turbine zaradi kavitacije in toka z delci predstavlja velik izziv pri hidroenergetskih sistemih, zlasti v rekah, bogatih s sedimenti. V tej študiji je predstavljena numerična raziskava vpliva trdnih delcev na erozijo rotorja Peltonove turbine. Simulacije računalniške dinamike tekočin (CFD) so bile izvedene z uporabo programa ANSYS CFX 2023 R2, pri čemer sta bila vključena Lagrangev pristop sledenja delcev in Finniejev model abrazije za napovedovanje erozijskih vzorcev pri različnih koncentracijah sedimentov. Rezultati kažejo, da pri običajnih pogojih sedimentacije erozija zaradi delcev ne prispeva bistveno k poškodbam konic lopatic. Vendar pa pri ekstremni obremenitvi s sedimenti napovedani erozijski vzorci tesno ustrezajo dejanskim opazovanjem, zlasti na konici lopatice.

Ključne besede Peltonova turbina, erozija zaradi trdnih delcev, kavitacija, CFD računalniška dinamika tekočin